Telescope Tasking for Maneuver Detection and Custody Maintenance using Evidential Reasoning and Reachability Theory

Daniel Aguilar Marsillach
University of Colorado Boulder
Marcus J. Holzinger
University of Colorado Boulder

ABSTRACT

This paper focuses on an autonomous tactical sensor tasking policy where specific hypotheses of interest are resolved using Dempster-Shafer theory. Optimal and unbiased hypothesis resolution is achieved by means of the Judicial Evidential Reasoning algorithm. Dynamical anomaly and custody hypotheses are resolved for a subset of station keeping GEO spacecraft. Evidence for anomaly and custody are quantified using Mahalanobis distance binary detection methods and reachability theory, respectively. Through a Monte Carlo design of experiments, the accuracy and robustness of the algorithm is studied to specified confidence levels. Lastly, the tasking algorithm is demonstrated in real-time on a Raven-class telescope.

1. INTRODUCTION

There is a warranted concern for the safety of current and future space-assets as a result of an increasing number of Earth-orbiting objects. To guarantee the safety of future space missions and operations, for commercial or scientific reasons, it is imperative to understand and predict how space object (SO) states evolve [1, 2]. To improve the decision-making processes, evidence of threats or hazards need to be identified in a timely manner. An area that could improve the detection of threats and hazards is that of telescope tasking. In particular, the above-mentioned goals motivate a need for predictive rather than reactive telescope tasking [3].

Early tasking methodologies optimize information theoretic measures to reduce global system uncertainty or state estimate covariances [4, 5]. The tasking problem has also been solved as a Markov Decision Process (MDP) in the information-space, using a receding-horizon control approach [6]. Linares and Furfaro formulate the optical tasking problem as an MDP that is solved using reinforcement learning to minimize system uncertainty [7]. A more recent method uses Rényi Divergence and labeled multi-Bernoulli filters to construct a reward function for multisensor tasking [8]. Lastly, a new survey strategy was developed that uses space object coverage and a weighted sky area approach to solve an optimization problem [9]. These strategies can be said to acquire observations that improve global state estimates which enable the resolution of unknown-unknowns by accumulating and post-processing a large amount of data [3]. Note that these strategies are more reactionary in nature. However, how one uses a suite of sensors to resolve known-unknowns, or predictive tasking, is of interest as it links SSA hypotheses directly to sensor management. DS theory is suitable for such tactical problems and is the focus of the presented telescope tasking problem solution, which is hypothesis-centric. Past work has been completed using Dempster-Shafer (DS) theory for tasking or decision-making problems [10, 11].

In [10], a general evidence-gathering algorithm that resolves hypotheses is introduced, using a cost function that reduces both non-specificity and ignorance, driving the algorithm to select actions that uniquely resolve the true element of the frame of discernment by minimizing by reducing using Jiroušek-Shenoy (J-S) entropy [10, 12]. This paper extends the capabilities of Judicial Evidential Reasoning (JER) and applies it to a real telescope system. Ensuring the successful implementation of such a tasking algorithm is multi-disciplinary and requires many components working together. JER is combined with estimation and reachability techniques to form a tasking algorithm that is able to evaluate and execute action sequences for optimal hypothesis resolution. In particular, the algorithm is updated to be purely driven by the system's belief states. Two important aspects related to the maintenance of space situational and domain awareness are the ability to maintain SO custody and discern dynamical anomaly. Custody maintenance is important for real-time status monitoring while inferring dynamical anomalies is required for object re-acquisition and

to conjunction event prevention. These two tasking objectives can be formulated in a frame of discernment using DS theory. To resolve these hypotheses, evidence for each has to be quantified.

This work redefines a Mahalanobis-distance binary detection method, specifically for Gaussian distributions, to quantify evidence for anomaly. Custody is quantified using position reachable set over-approximations and is maintained for a narrow-FOV telescope if the position reachable set approximation is contained in the telescope's FOV. If the reachable set is not fully contained in the FOV, there exists a possibility that custody has been lost, favoring a search through the reachable set. The over-approximation is obtained by finding the maximal radius of the position reachable set and is updated for each SO in the observation campaign using continuation methods. The result is a telescope tasking algorithm that is driven to maintain custody by preventing position reachable sets from becoming too large while simultaneously detecting maneuvers.

A Monte Carlo study is designed and implemented to determine the accuracy and robustness of the algorithm to a specified statistical confidence level. SOs in the public SO catalog are modeled to perform aggressive North-South (NSSK) and East-West (EWSK) station keeping. With the use of confusion matrices, false-positive and false-negative classification rates are quantified. In terms of anomaly detection, it is found that reducing false-negative rates is most desirable for custody maintenance. Results show custody is maintained for all observable spacecraft in the Monte Carlo simulation.

In addition to presenting robustness in simulation, a successful and empirical real-time demonstration of the JER tasking algorithm is shown for a Raven-class telescope. This requires several working hardware and software subsystems. A telescope infinite-horizon LQR mount controller is used to open-loop track TLEs from the public catalog using TheSkyX Software. Image processing is used to background subtract, detect, track, and discriminate SOs of interest through the use of blob detection and a GM-PHD multi-target tracking algorithm. Topocentric right ascension and declination measurements are used with an Unscented Kalman Filter to estimate SO inertial states. The real-time demonstration resolves the custody and anomaly hypotheses for a combination of North-South and East-West station keeping GEO satellites.

This paper contains a number of contributions relating to the application and extension of the JER tasking algorithm for space situational awareness. First, a new maneuver detection method using Mahalanobis distance is presented. Second, new evidence to hypothesis belief mappings are formulated that result in a purely belief and reachability driven algorithm. Third, the robustness of the algorithm is demonstrated through a Monte Carlo simulation given specified confidence interval significance levels, that evaluates success and fail rates. Lastly, the algorithm is interfaced with existing observatory hardware to resolve the listed hypotheses using optical data in real-time.

2. THEORY

2.1 Dempster-Shafer Evidential Reasoning

An advantage of DS theory is its ability for reasoning with epistemic uncertainties, as one can model degrees of support for a particular proposition, given a piece of evidence. This can simplify decision-making by using Dempster's combination rule for aggregating independent pieces of evidence [13]. The theory allows one to pose and resolve a hypothesis mathematically as well as model complete ambiguity and equally likely propositions differently.

Hypotheses can be formulated mathematically using the frame of discernment, that is, the available state-space of a variable denoted by Θ. The elements of the power set of Θ, 2^Θ, or the set of all subsets, are referred to as propositions. By definition, the allowable state variables in the frame of discernment have to be mutually exclusive and collectively exhaustive, implying that only one element of the frame of discernment can be true [13]. For a given frame of discernment, Θ, the basic probability assignment (BPA) function m assigns degrees of belief or support to particular elements of the power set 2^Θ and is defined as

$$m : 2^\Theta \mapsto [0,1] \tag{1}$$

$$m(\emptyset) = 0 \tag{2}$$

$$\sum_{a \in 2^\Theta} m(a) = 1. \tag{3}$$

The constraint in (3) enforces the mutually exclusive and collectively exhaustive property. The quantity $m(a)$ is the basic probability mass of set a, and is interpreted as the belief assigned exactly to a, not its subsets. Additionally, (2) enforces that no belief is committed to the null set.

Two BPAs m_1 and m_2, representing distinct pieces of evidence, can be combined to form a new aggregate BPA $m_1 \oplus m_2$ using Dempster's combination rule [14]:

$$(m_1 \oplus m_2)(a) = K^{-1} \sum_{b_1, b_2 \in 2^\Theta \,:\, b_1 \cap b_2 = a} m_1(b_1) m_2(b_2) \tag{4}$$

where K is a normalization constant given by:

$$K = 1 - \sum_{b_1, b_2 \in 2^\Theta \,:\, b_1 \cap b_2 = \emptyset} m_1(b_1) m_2(b_2) \tag{5}$$

Using DS theory, the anomaly hypothesis is defined with the following frame of discernment:

$$\Theta_A = \{N, \mathscr{A}\}, \tag{6}$$

where N and $\mathscr{A}$ denote nominal and anomalous, respectively. The power set of the frame is:

$$2^{\Theta_A} = \{\emptyset, \{N\}, \{\mathscr{A}\}, \{N, \mathscr{A}\}\} \tag{7}$$

Similarly, the custody frame of discernment is paramaterized by C, denoting custody, such that

$$\Theta_C = \{C, \neg C\}, \tag{8}$$

where its corresponding power set is

$$2^{\Theta_C} = \{\emptyset, \{C\}, \{\neg C\}, \{C, \neg C\}\}. \tag{9}$$

As mentioned, the power set denotes the propositions for each frame of discernment and DS theory allows one to specify probability mass directly to elements of these sets of all subsets. Pieces of evidence are then used to obtain the true anomaly or custody status in the frame of discernment.

2.2 Judicial Evidential Reasoning

Fundamentally, JER evaluates and selects actions that best resolve a set of hypotheses. The algorithm iteratively evaluates action paths that gather multiple pieces of evidence to resolve hypotheses to a reasonable tolerance [10]. Different decision paths are compared to each other via an appropriate cost function. In this work, Jiroušek-Shenoy (J-S) entropy, which is interpreted as a measure of total uncertainty in a BPA, is used. J-S entropy is maximum for vacuous BPAs that represent complete ambiguity or ignorance, which occurs when all of the belief mass is given to the frame of discernment such that $m(\Theta) = 1$, representing a complete lack of knowledge of which element $a \in \Theta$ is true. Minimizing J-S entropy is directly equivalent to identifying the true proposition in a frame of discernment. J-S entropy then becomes an appropriate measure, or objective function, to be minimized for the purposes of hypothesis resolution.

We can use multiple hypotheses, or frames of discernment, resulting in the set $\tilde{\Theta} = \{\Theta_1, ..., \Theta_h\}$, where Θ_h is an individual hypothesis of size $|\Theta_h|$. A discrete-time set, $t = \{t_k,\ t_{k+1}, ...,\ t_{k+T}\}$, is considered at which sensor actions can be taken. The set of available actions at time t_i for sensor j are given by the following index set $\mathbb{A}_{j,t_i} = \{1, \ldots, n_{A,j}\}$, where $n_{A,j}$ is maximum number of available actions. Under the assumption that a given sensor can only perform one action at a time, the available actions for sensor j throughout the time horizon $t_i \in \{t_k, \ldots, t_{t+T}\}$ is

$$\mathbb{A}_j = \mathbb{A}_{j,t_k} \times \cdots \times \mathbb{A}_{j,t_{k+T}}. \tag{10}$$

Given a sensor network, the set containing all possible action sequences of the network is obtained by taking the Cartesian product of (10) over all sensors, s, yielding

$$\mathfrak{A} = \mathbb{A}_j \times \cdots \times \mathbb{A}_s. \tag{11}$$

Generally, the objective is to obtain the action set, $A \in \mathfrak{A}$ for s sensors that minimizes the J-S entropy, H_{JS}, which is a function of the states in the frames of discernment. Additionally, a weight, w_h, is designated to specify the priority for resolving particular hypothesis Θ_h. As such, the optimal action sequence for the network of sensors is given by

$$A^* = \underset{A \in \mathfrak{A}}{\arg\min} \sum_{h=1}^{|\tilde{\Theta}|} w_h H_{js}(\Theta_h),\ \Theta_h \in \tilde{\Theta} \tag{12}$$

Actions lead to pieces of evidence in the form of observations and processed data. When the evidence is combined using the conjunction rule, an accrued evidence BPA can be computed. Suppose the prior BPA is denoted $m_h^-(t_k)$ BPA, $\tilde{m}_h(t_k)$ is the accrued evidence at time t_k related to hypothesis h, combination of these BPAs leads to a posterior BPA $m_h^+(t_k)$

$$m_h^+(t_k) = m_h^-(t_k) \oplus \tilde{m}_h(t_k). \tag{13}$$

Multiple pieces of evidence can be gathered at a single time index if multiple sensors are used. A given sequence α directly leads to sets of evidence. Since optimizing (12) is non-trivial, the original formulation is broken down into a sub-problem using adversarial optimization for computational tractability. An efficient action tree is constructed using alpha-beta pruning. An alternating agent approach is adopted using minimax and maximin optimization [10]. By finding and implementing action sequences that are proposition selfish, one gives equal opportunity to opposing agents to build a case for or against a particular proposition. This approach reduces confirmation bias and limits convergence to erroneous propositions. More details regarding JER can be seen in Jaunzemis' prior work [10].

To capture the changing belief states over time, the JER algorithm is implemented using a receding time-horizon approach. Consequently, the first actions in $\tilde{\alpha}^*$ are implemented and the full process is repeated again for the next time step. The actions change the next iteration's initial conditions, providing the necessary feedback for the algorithm to resolve all of the hypotheses.

2.3 Binary Hypothesis Detection

Given a reference trajectory, a state estimate, and associated PDFs, deviations between the estimates and the reference can be used to quantify evidence for the anomaly hypothesis, which can be caused by un-modeled perturbations or maneuvers. This hypothesis is particularly important as SOs in anomalous orbits can compromise the safety of other active assets. Let the null and alternate hypotheses be denoted by $\mathscr{H}_0$ and $\mathscr{H}_1$, respectively. If the PDFs of these hypotheses are known, a pre-defined false alarm level, γ, allows one to perform a binary hypothesis test to detect anomalies [15].

The purpose of anomaly detection in this paper serves to identify maneuvers or mismodeled dynamics. The null hypothesis is modeled by a nominal (non-maneuvered) PDF, $f_n(\boldsymbol{x}_n(t);\ p)$, which is constructed from an uncorrelated track (UCT) at time t_0. This can also be constructed from the last available state PDF. Conversely, the anomalous (maneuvering) PDF is given by $f_a(\boldsymbol{x}_a(t);\ p)$, and is constructed by successively updating the nominal PDF with measurements via the UKF. Under the Gaussian assumption, it is only of interest to estimate the first two moments of each PDF via the unscented transform [16]. Figure 1 demonstrates the various possiblilities, where there are two SO state distributions, given by uncorrelated tracks at t_0, which diverge from the nominal trajectory by different amounts. SO 1 in the diagram is likely nominal, due to a large overlap in the nominal and anomalous PDFs, whereas SO 2 is likely anomalous due to the reduced overlap in the Null and alternate hypothesis PDFs.

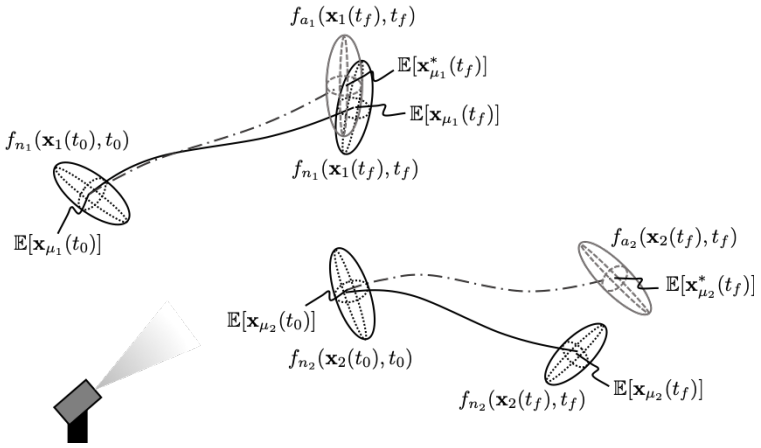

Fig. 1: Illustration of telescope tasking for anomaly resolution. One spacecraft is nominal and the other is anomalous, as per binary hypothesis detection methods.

Consider the random vectors $\boldsymbol{x}_n, \boldsymbol{x}_a \in \mathbb{R}^6$, representing the nominal and anamolous true state vectors of an SO. Under the null hypothesis $\mathscr{H}_0$, one expects the anomalous and nominal random vectors to be similar, because there is no

statistical evidence that would suggest a dynamical anomaly has occurred, so

$$\boldsymbol{x}_n(t) \approxeq \boldsymbol{x}_a(t) \tag{14}$$

Another random vector can be defined as

$$\boldsymbol{\Delta} = \boldsymbol{x}_n(t) - \boldsymbol{x}_a(t). \tag{15}$$

If the assumptions for the nominal and anomalous random vectors are assumed to be Gaussian, the PDF of $\boldsymbol{\Delta}$ is

$$\boldsymbol{\Delta} \sim N\big(\ \mathbb{E}[\boldsymbol{x}_n(t)] - \mathbb{E}[\boldsymbol{x}_a(t)],\ P_n + P_a\big) \tag{16}$$

As such, under the null hypothesis, one expects this random vector have the following distribution:

$$\boldsymbol{\Delta} \sim N\big(\ \mathbf{0}_{6\times 1},\ 2P_n\big). \tag{17}$$

If the alternate hypothesis is true, then the expected value $\mathbb{E}[\boldsymbol{\Delta}] \neq \mathbf{0}_{6\times 1}$ and $P_n \neq P_a$. As such, in a similar fashion to [15], Mahalanobis distance (MD) can be used to construct a scalar PDF to compare the $\mathscr{H}_0$ and $\mathscr{H}_1$ PDFs.

Using the PDF in (17), random vectors can be sampled, yielding $\boldsymbol{\Delta}_i$, under the assumption the Null hypothesis is true. Then, the following MD can be computed for each sample

$$d_{i|\mathscr{H}_0} = \left(\big(\boldsymbol{\Delta}_i - \mathbb{E}[\boldsymbol{\Delta}|\mathscr{H}_0]\big)^\top \ (2P_n)^{-1} \ \big(\boldsymbol{\Delta}_i - \mathbb{E}[\boldsymbol{\Delta}|\mathscr{H}_0]\big) \right)^{\frac{1}{2}}. \tag{18}$$

where, $\mathbb{E}[\boldsymbol{\Delta}|\mathscr{H}_i]$ is the expected value of $\boldsymbol{\Delta}$, given the Null hypothesis is true. Similarly, the MD of a random vector sampled from the alternate hypothesis PDF in (16) is desired, which are denoted $\tilde{\boldsymbol{\Delta}}_i$. Then the MD of these samples with respect to the Null hypothesis is computed using

$$d_{i|\mathscr{H}_1} = \left(\big(\tilde{\boldsymbol{\Delta}}_i - \mathbb{E}[\boldsymbol{\Delta}|\mathscr{H}_1]\big)^\top \ (2P_n)^{-1} \ \big(\tilde{\boldsymbol{\Delta}}_i - \mathbb{E}[\boldsymbol{\Delta}|\mathscr{H}_1]\big) \right)^{\frac{1}{2}}. \tag{19}$$

With enough samples, numerical PDFs for the null and alternate hypotheses, $f_0(d)$ and $f_1(d)$, respectively, are constructed in terms of MD d. Thus, a binary hypothesis test can be performed given a pre-defined significance level. The probability of false-alarm and detection can be computed numerically as:

$$p_{fa} = \int_{\nu}^{\infty} f_n(s)ds \tag{20}$$

$$p_d = \int_{\nu}^{\infty} f_a(s)ds, \tag{21}$$

where $\nu \in \mathbb{R}_{\geq 0}$ represents the Mahalanobis distance variable at a given significance level $\gamma \in (0,1]$. Then, if $p_d > p_{\text{thresh}} = 1 - P_{FN}(\gamma)$, the null hypothesis is rejected for the alternate hypothesis. We define the binary variable p_n such that

$$p_n = \begin{cases} 0, & p_d \leq p_{\text{thresh}} \\ 1, & p_d > p_{\text{thresh}}, \end{cases} \tag{22}$$

which is used for quantifying evidence later using Dempster Shafer theory. Note that (18) will be Chi-squared by definition with degree of freedom $k = 6$, though (19) is not. As $\mathbb{E}[\boldsymbol{\Delta}] \to 0$ and $P_a \to P_n$, the binary hypothesis test indicates a state is nominal.

2.4 Spacecraft Reachability

Custody maintenance requires having an understanding of when an SO is performing a maneuver and accurately modeling the dynamics of such an object. A poor understanding of dynamics can result in loss of custody. Similarly, if an object maneuvers, which is a special case of mismodeled dynamics, custody can also be lost as the object cannot be tracked with appropriate observation instruments. One way of compensating for such a lack of knowledge is by computing hypothesized forward reachable sets of the object under the assumption of a control policy. In this paper, the SOs of interest are geostationary (GEO) satellites, in almost circular orbits with very low inclinations. For a

pre-specified time-horizon, an initial condition $\boldsymbol{x}_0$, and an admissible control set $\mathscr{U}$, the reachability problem can be expressed as an optimal control problem of the following form

$$\begin{aligned} \max_{\boldsymbol{u}\in\mathscr{U}} \quad & \frac{1}{2}\boldsymbol{x}_f^\top G\boldsymbol{x}_f \\ \text{s.t.} \quad & \dot{\boldsymbol{x}} = \boldsymbol{f}(\boldsymbol{x},\boldsymbol{u},t) \\ & g(\boldsymbol{x}_0,t_0) = 0, \end{aligned} \tag{23}$$

where the initial manifold $g(\boldsymbol{x}_0,t_0)$, in this paper, is given by an ellipsoidal set. The resulting forward position reachable set, the set of all possible states a system can have given an initial set and a specified time-horizon, is formally defined as

$$\mathscr{R}(t_f;\mathscr{U},\boldsymbol{f},g,t_0) = \{x_f \in \mathbb{R}^n :\ \forall \boldsymbol{u}(t) \in \mathscr{U},\ g(\boldsymbol{x}_0) \leq 0,\ \boldsymbol{x}_f = \phi_x(t_f;\boldsymbol{x}_0,\boldsymbol{p}_0,t_0),\ t \in [t_0,t_f]\}. \tag{24}$$

As a result, any state outside of the forward reachable set is not physically attainable by the system with the admissible controls $\mathscr{U}$. In this paper, the set given by (24) is over-approximated for the purposes of telescope tasking, by means of a 6-dimensional sphere [17]. By assuming that a maneuvering or non-maneuvering spacecraft is using optimal control to maximize the reachable distance from some initial set, we are tasking telescopes for a worst case scenario.

Instead of computing the entire position reachable set, in this work, we compute the reachable distance along a pre-specified direction. Then, numerical continuation is used to update this maximum reachable distance as a function of the time-horizon, T, which amounts to integrating a set of differential equations [18]. The existence of a maximal radius for the position reachable set, given a pre-specified time-horizon, is established in [17]. Thus, the maximum reachable distance along $\hat{\boldsymbol{d}}_s$ is $d_f = \|H(\boldsymbol{x}_f - \boldsymbol{0}_{6\times1})\| = \|H\boldsymbol{x}_f\|$, where $H = [I_{3\times3}, 0_{3\times3}]^\top$ is the matrix that projects the 6-dimensional states onto the position subspace. Given a bounded radius d_f, an over-approximation of the position reachable set is constructed by the set

$$B_{d_f}(\boldsymbol{x}) = \{\boldsymbol{x} \in \mathbb{R}^6 \ :\ \|H\boldsymbol{x}\| \leq d_f\}. \tag{25}$$

Hence, if the position subspace is denoted by $\mathscr{P} \subseteq \mathbb{R}^3$, then

$$\text{proj}_{\mathscr{P}}(\mathscr{R}) = \{\boldsymbol{y} \in \mathbb{R}^3 : \boldsymbol{y} = H\boldsymbol{x},\ \forall \boldsymbol{x} \in\ \mathscr{R}(t_f;\mathscr{U},\boldsymbol{f},g,t_0)\}. \tag{26}$$

It is easily shown that $\text{proj}_{\mathscr{P}}(\mathscr{R}) \subset \text{proj}_{\mathscr{P}}(B_{d_f})$, i.e. the position reachable set is wholly contained in (25). This is particularly useful as a bounded set can be searched to maintain custody of an SO. For each SO, numerical continuation is used to update (25) as a function of time horizon.

2.5 Reachability-based Custody BPA

The position reachable set is the projection of the full-state reachable set onto the position subspace, even though velocity variables are still considered in the reachable set computation. In this paper, only the position subspace is relevant for a telescope trying to observe the spacecraft. The velocity at a given moment may be important for the anomaly detection, but the position reachable set is what matters for maintaining custody. This section discusses how the reachable set over-approximation relates to custody maintenance.

Given the telescope's FOV, paramaterized by angle θ, and the estimated range vector from a ground station to the spacecraft

$$\boldsymbol{\rho} = \hat{\boldsymbol{x}} - \boldsymbol{x}_{gs} \tag{27}$$

the maximum distance a telescope can view away from $\hat{\boldsymbol{x}}$, i.e. the estimated trajectory, along the sensor plane is

$$d_{FOV} = ||\boldsymbol{\rho}||\sin(\theta). \tag{28}$$

Clearly, the scalar $d_{FOV} \in \mathbb{R}_{\geq 0}$ is a function of the range vector. For high altitude orbits, d_{FOV} is large since a large vector is swept by angle θ, whereas for low altitude orbits, d_{FOV} is small. In this paper, a new definition of custody is introduced, such that when the position reachable set is projected onto the image plane, if it is wholly contained in the telescope FOV, custody is guaranteed over that time-interval. In other words, no portion of the reachable set lies outside of the FOV. The area of the projection of the over-approximated reachable set $B_{d_f}(\boldsymbol{x})$ onto the sensor plane is then given by $A_r = \pi d_f^2$. When $d_f > d_{FOV}$, a portion of the projected reachable set lies outside the FOV, as seen in Figure 2b. Conversely, when $d_f < d_{FOV}$, this indicates that the reachable set is fully contained in the FOV, hence

$A_r \leq A_{FOV}$, where A_{FOV} is the area of the FOV on the image plane computed using (28). This is shown in Figure 2a. The areas can be computed by projecting each set onto the the image (sensor), which is then used to determine the degree of custody a telescope has with respect to an SO and its position reachable set. Hence, the area of this projected set is

$$A_{r,out} = \begin{cases} 0, & A_r < A_{FOV} \\ A_r - A_{FOV}, & A_r > A_{FOV}. \end{cases} \tag{29}$$

Naturally, the larger $A_{r,out}$ becomes, the less likely custody can be maintained i.e. as $A_{r,out} \to \infty$, $p_c \to 0$. Conversely, $A_{r,out} = 0$ suggests the probability mass for custody, $p_c = 1$. As such, an area-based basic probability mass measure, $p_c \in [0,1]$, is constructed that represents the degree to which custody is maintained, summarized by the following equation

$$p_c = \begin{cases} 1, & A_r < A_{FOV} \\ \frac{A_{r,out}}{A_r}, & A_r > A_{FOV}. \end{cases} \tag{30}$$

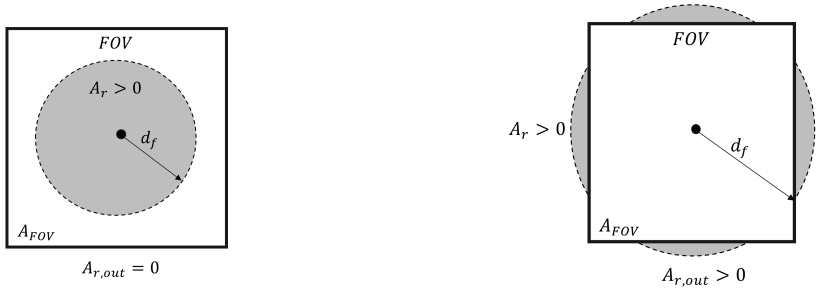

(a) $A_{r,out} = 0$: Full custody probability mass

(b) $A_{r,out} > 0$: Reduced custody probability mass

Fig. 2: Custody Scenarios Based on Maximum Reachable distance d_f

2.6 Evidence to Hypothesis Mappings

One of the goals of the paper is to ensure that the size of each spacecraft's reachable set drives the tasking algorithm to perform different actions. The telescope's FOV will determine how many distinct actions are required. If multiple objects of interest can be seen in one image, less independent actions are required to resolve their hypotheses. It is assumed that each telescope has two available actions, namely, tracking or searching for an SO of interest. If there are N SOs of interest, then the action at time t_i for a given sensor j, is a function

$$\mathbb{A}_{j,t_i} = \{\emptyset, T, S\}, \tag{31}$$

where track action, T, results in the telescope tracking and observering the nominal trajectory of a desired spacecraft through the use of the predicted estimates. The search action, S, searches the over-approximated reachable set. This search occurs around the nominal (predicted) trajectory, since the reachable set is computed in terms of relative states with respect to the estimate mean.

The impact a given action has on the belief state needs to be quantified. We have already quantified the probability mass p_c that custody can be maintained in (30), which is the custody probability conditioned on the SO being on a nominal trajectory. This occurs when a tracking action is chose, such that $p_c \equiv p_{c|T}$. The alternative is the custody probability conditioned on a search action, $p_{c|S}$. By definition, the state of the SO should be a member of the over-approximated reachable set, thus, searching the reachable set leads to custody re-acquisition, hence $p_{c|S} = 1$. As such, $p_{c|T} \leq p_{c|S} = 1$, which makes searching a desirable action when $p_{c|T} << p_{c|S}$. This probability measure is used to create a BPA for the custody hypothesis that depends on the action taken in $\mathbb{A}_{j,t_i}$. Additionally, the probability measure is scaled by the probability of detecting an SO in optical data, p_d [19].

2.6.1 Planning BPAs

The BPAs in the planning phase use the custody probability mass to form a gain-scheduling method to appropriately select tracking or searching actions. The BPA must adhere to (1) [13]. For a given custody hypothesis $\Theta_C \in \tilde{\Theta}$ the planning BPA is

$$\begin{aligned} \hat{m}^-_{c|T}(\{C\}) &= p_d\ p_{c|T}, & \hat{m}^-_{c|S}(\{C\}) &= p_d\ (p_{c|S} - p_{c|T}) = p_d\ (1 - p_{c|T}), \\ \hat{m}^-_{c|T}(\Theta_C) &= 1 - \hat{m}^-_{c|T}(\{C\}), & \hat{m}^-_{c|S}(\Theta_C) &= 1, -\hat{m}^-_{c|S}(\Theta_C), \end{aligned} \tag{32}$$

where $\hat{m}^-_{c|\cdot}$ denotes the BPA affecting the custody hypothesis given a particular planned action. These BPAs encode the impact of a tasking action on the custody hypothesis. The custody search action BPA is constructed such that when $p_{c|T}$, is low, search actions are prioritized. Conversely, when $p_{c|T}$ is high, search actions are minimized, as they reduce JS entropy less than tracking actions, resulting in a gain-scheduling-like method to prioritize certain actions at different times.

On the other hand, when resolving the anomaly hypothesis, the size of the over-approximated reachable set does not provide any indication of whether or not an anomaly may have occurred, as such, the probability measure that an SO is nominal, $p_n = p_{n|T} = p_{n|S}$. Thus, given an anomaly hypothesis $\Theta_A \in \tilde{\Theta}$, the planning anomaly BPA is

$$\begin{aligned} \hat{m}^-_{a|T}(\{N\}) &= p_d\ p_n\ p_{c|T} & \hat{m}^-_{a|S}(\{N\}) &= p_d\ p_n\ (1 - p_{c|T}) \\ \hat{m}^-_{a|T}(\{A\}) &= p_d\ (1 - p_n) p_{c|T} & \hat{m}^-_{a|S}(\{A\}) &= p_d\ (1 - p_n)(1 - p_{c|T}) \\ \hat{m}^-_{a|T}(\Theta_A) &= 1 - \hat{m}^-_{a|T}(\{N\}) - \hat{m}^-_{a|T}(\{A\}), & \hat{m}^-_{a|S}(\Theta_A) &= 1 - \hat{m}^-_{a|S}(\{N\}) - \hat{m}^-_{a|S}(\{A\}) \end{aligned} \tag{33}$$

where $\hat{m}^-_{a|\cdot}$ denotes the BPA affecting the anomaly hypothesis given a particular action, p_d, p_c, and p_n are the probability of detecting an SO in a given image, the probability of maintaining custody, and the probability of an SO being nominal, respectively. Not that unless $p_d = p_c = p_n = 1$, belief is always given to the frame of discernment Θ.

2.6.2 Execution BPAs

When an action is selected and executed in a receding-horizon manner, the evidence has to be quantified in terms of a coherent BPA. Then, the gain-scheduling terms are removed as the evidence quantification is the same whether a tracking or search action is chosen i.e. the evidence is purely a function of acquired measurements, which leads to

$$\begin{aligned} \hat{m}^+_{c|T}(\{C\}) &= p_d & \hat{m}^+_{a|T}(\{A\}) &= p_d\ (1 - p_n) \\ \hat{m}^+_{c|T}(\Theta_C) &= 1 - \hat{m}^+_{c|T}(\{C\}), & \hat{m}^+_{a|T}(\Theta_A) &= 1 - \hat{m}^+_{a|T}(\{N\}) - \hat{m}^+_{a|T}(\{A\}) \\ \hat{m}^+_{c|S}(\{C\}) &= p_d & \hat{m}^+_{a|S}(\{N\}) &= p_d\ p_n \\ \hat{m}^+_{c|S}(\Theta_C) &= 1 - \hat{m}^+_{c|S}(\Theta_C) & \hat{m}^+_{a|S}(\{A\}) &= p_d\ (1 - p_n) \\ \hat{m}^+_{a|T}(\{N\}) &= p_d\ p_n & \hat{m}^+_{a|S}(\Theta_A) &= 1 - \hat{m}^+_{a|S}(\{N\}) - \hat{m}^+_{a|S}(\{A\}) \end{aligned} \tag{34}$$

where $\hat{m}^+_{c|\cdot}$ and $\hat{m}^+_{a|\cdot}$ denote the BPAs affecting the custody and anomaly hypotheses, respectively,given a particular executed action. It should be noted that in this work, no basic probability mass is given to the no custody proposition, $\neg C$, which forces the algorithm to always maintain custody of the desired SOs.

3. METHODOLOGY

3.1 Monte Carlo Study

To test the robustness of the algorithm to varying cases of anomaly, a Monte Carlo study is completed. For this study, like the demonstration, initial orbit data is acquired from the Space Track catalog [20]. Only one input is varied, namely, each SOs assumed maneuver duration T. This represents the time-horizon a spacecraft uses optimal control to maximize its reachable distance in the along-track, $\hat{\boldsymbol{o}}_\theta$, and cross-track directions, $\hat{\boldsymbol{o}}_h$, which are related to East-West

(EWSK) and North-South (NSSK) station keeping maneuvers. This represents a realistic scenario current ground stations have to face.

However, in this paper, the maneuvers are modeled to be more aggressive since in traditional operations, spacecraft do not use optimal control to maximize the reachable distance in the along-track, $\hat{\boldsymbol{o}}_\theta$, or cross-track, $\hat{\boldsymbol{o}}_h$, direction, to perform EWSK or NSSK. Instead, it is assumed that each spacecraft is continuously maneuvering to maximize its reachable distance from its nominal trajectory. By sampling maneuver times, the reachable set is effectively sampled to initialize anomalous spacecraft.

The most important outcome of the simulation is to determine classification accuracy. For statistical classification tasks, there are various measures of performance, succinctly summarized by a confusion or error matrix. A typical measure is accuracy, defined as:

$$\text{Accuracy} = \frac{\text{TP}+\text{TN}}{\text{TP}+\text{TN}+\text{FP}+\text{FN}}, \tag{35}$$

where TP, TN, FP, and FN are the true positive, true negative, false positive, and false negative rates of the experiment. Accuracy represents the ratio of successful classifications to number of trials. To get a statistical strength on the Monte Carlo's measurement of accuracy, a minimum number of experiments or trials are required. In particular, denote accuracy by $\hat{p}$, like the probability of success in a Bernoulli trial. It is reasonable to assume that $\hat{p}$ will be normally distributed, by the law of large numbers. As such, given a desired confidence interval width, w, and a significance-level α, $z_{\frac{\alpha}{2}}$ can be found for a standard normal distribution. Then, the required number of runs is

$$n_{MC} = \left(\frac{z_{\frac{\alpha}{2}}}{w}\right)^2 \left(\hat{p}-\hat{p}^2\right) \tag{36}$$

where w is the desired half-width of the confidence interval, $\hat{p}$ is the estimated accuracy, and $z_{\frac{\alpha}{2}}$ is the $\frac{100\alpha}{2}$ percentage point of the standard normal distribution [21]. The number of Monte Carlo runs, n_{MC}, depends on the expected accuracy. Note that $\hat{p}=0.5$ maximizes the number of runs, so this is used to get an upper bound on the necessary trials. If $w=0.02=2\%$, $\alpha=0.05$, $z_{\frac{\alpha}{2}}=1.96$, and thus, $n_{MC}=2412$. For each JER simulation, the ground station is tasked to resolve two hypotheses for 12 SOs at a time. This leads to 201 necessary JER simulations.

The assumed maneuver duration T is sampled from a uniform distribution $T^{(i)} \sim U[T_l,\ T_u]$, where T_l, and T_u are the lower and upper bounds of the time-horizon uniform distribution, and are chosen to be $T_l = 10$ min. and $T_u = 4$ hours. In this simulation, it is assumed that T_u hours have elapsed since the satellites were last observed by another ground station. By using the prior covariance ellipsoid as the initial set, the ground stations reachable sets are computed at the time the JER tasking algorithm is initialized, and again, T_u is used to constrain the maximum size of each reach set. Table 1 highlights a summary of the MC related parameters. Since continuous-time optimal control is used to compute the position reachable set over-approximations, the thrust capability, parameterized by u_m, is chosen for an electric-propulsion class spacecraft with a mass between $500-1000$kg.

Table 1: Monte Carlo Parameters

n_{sim}	T_l (Hours)	T_u (Hours)	u_m (km/s^2)	P_{FA}
201	0.17	4	1×10^{-8}	[0.05, 0.1, 0.15]

As mentioned in section 2.3, a non-maneuvering (quiescent) PDF and the updated estimate's PDF are used to discern anomaly using a binary hypothesis detection method. Since the PDFs are assumed to be Gaussian, their mean and covariance matrix are required to fully characterize the PDFs and use the anomaly detection method. Both the nominal (non-maneuvering) and estimate covariances, P_n, and P_a are initialized with position variance σ_p and velocity variance σ_v, yielding:

$$P_n = P_a = diag(\ \sigma_p^2\ \mathbf{1}_{1\times3},\ \sigma_v^2\ \mathbf{1}_{1\times3}\ ) \tag{37}$$

where $\sigma_p = 15\ km$ and $\sigma_v = 2\ ms^{-1}$. The remainder of the paper assumes that $\hat{P}^+ = P_a$. The true state for SO i is sampled from the 2σ covariance ellipsoid centered at the state estimate mean, such that

$$\boldsymbol{x}_{so,i} \sim \mathcal{N}\left(\hat{\boldsymbol{x}}_i^+, \hat{P}_{2\sigma,i}^+\right). \tag{38}$$

The σ_p^2 and σ_v^2 values are chosen to be related to nominal Geostationary slot sizes, which are nominally separated by some minimum angular separation, resulting in a Cartesian separation of roughly 100km. Then, σ_p is chosen such that $3\sigma_p \sim 100$ km. Thus, the nominal PDF assumes that spacecraft are in their respective GEO slot. For the purposes of the Monte Carlo study, it is assumed that the i^{th} SO's nominal reference trajectory is centered in its GEO slot and the true states are thus sampled from the interior of the GEO slot.

3.2 Hardware

For this particular demonstration, a Raven-class telescope called the Georgia Tech-Space Object Research Telescope (GT-SORT), located in Midtown, Atlanta, Georgia, USA, is used. Software Bisque's Paramount ME II telescope mount is used to control the pointing with TheSkyX Professional Edition software. Interfacing the JER code and incorporating telescope and camera control modules requires custom made scripts developed in Python. Two optical sensors are used, namely, the ZWO AS I071MC Pro (color) and ZWO ASI174MM-Cool (mono) cameras. The cameras are used for the telescope and finderscope, respectively.

Regardless of whether a search or track action is selected, images (observations) are taken with the main telescope and finderscope cameras. These are processed to acquire RADEC measurements, which are fed to each SOs UKF. Table 2 shows the GT-SORT and finderscope optical performance characteristics.

Table 2: Electro-Optical Sensor Parameters

Sensor	Focal Ratio	FOV (arcmin.)	iFOV (arcsec.)	Lim. Mag.
Telescope	f/6	25.56 x 16.98	0.31	12.9
Finderscope	f/2	287.58 x 181.38	8.127	12.06

A summarized process highlighting the JER algorithm for the demonstration is presented in Figure 3. This purposely resembles a control flow diagram, where the actions are based on the current belief states. The receding horizon approach results in the first action being selected and executed. The measurements over an action interval are used to quantify the evidence as highlighted in section 2. A BPA is formed for each piece of evidence, which are then combined, updating the belief states for each hypothesis. After initialization, the observation campaign ends when all of the hypotheses are resolved, or, the JS entropies are below a pre-defined threshold [22]. For additional details on the hardware implementation, see [22, 23].

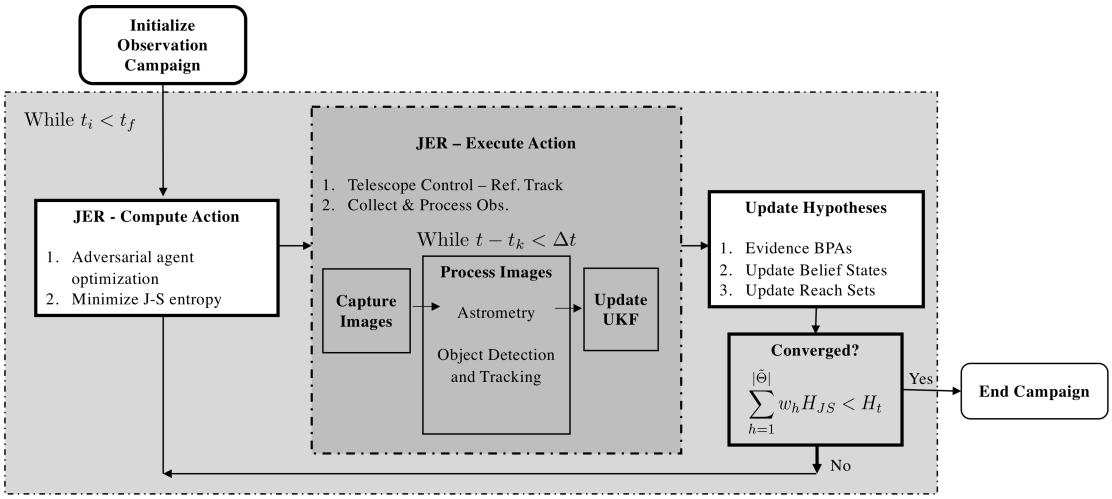

Fig. 3: Hardware/Software Telescope Logic

Moreover, the light pollution in the city makes star detection challenging with narrow FOV telescopes see Figure 7b, which has limited star streak detections and noise in the center of the frame. In contrast to telescope rate-tracking, SO or object tracking must be done from image frame to frame using a Gaussian-Mixture Probability Hypothesis Filter [24], readily available from previous lab projects, to detect and track the object between measurements. This is a high

SNR multi-object tracking algorithm that uses multiple particle filters to track objects across several image frames. Once a measurement is obtained, the pixel-coordinates of the SO are mapped to the finder scope's pixel coordinates.

4. RESULTS

The results obtained from the theory and hardware contributions are discussed in this section. Initially, a specific simulation from the Monte Carlo batch is presented. Subsequently, the general outcomes from the Monte Carlo study are discussed and lastly, the results obtain in the empirical demonstration are shown.

4.1 Specific Simulation Case

In this simulation, the ground station is tasked to resolve the anomaly and custody hypotheses for 12 SOs, all of which, are initialized as vacuous or fully ambiguous, hence $H_{js}(\Theta_h) = 1,\ \forall \Theta_h \in \tilde{\Theta}$. The corresponding receding-horizon, or executed, tasking schedule can be seen in Figure 4. The two types of action at any given action interval are labeled as 'Track' or 'Search' in green and red, respectively. The observation campaign starts at 02:57:00 UTC and ends at 04:57:00 UTC, lasting a total of 4 hours. When the JER algorithm converges and resolves all of the hypotheses, no further actions are necessary, hence the telescope is 'Idle' for the remainder of the time-horizon.

The result of the gain-scheduling clearly takes effect, hence first search actions are used on spacecraft with very large d_f. Using (28), if the telescope's FOV is parameterized by $\theta \approx 0.283°$, for SOs in GEO, one obtains $d_{fov} \approx 172$km. As such, when $d_f \leq d_{fov}$, when the over-approximated reach set is fully contained in the FOV, tracking actions are selected. Conversely, when $d_f > d_{fov}$, which implies $A_{r,out} \neq 0$, search actions are selected, which can be seen in Figure 4. The maximum reachable set radius as a function of time for each spacecraft is visible in Figure 5.

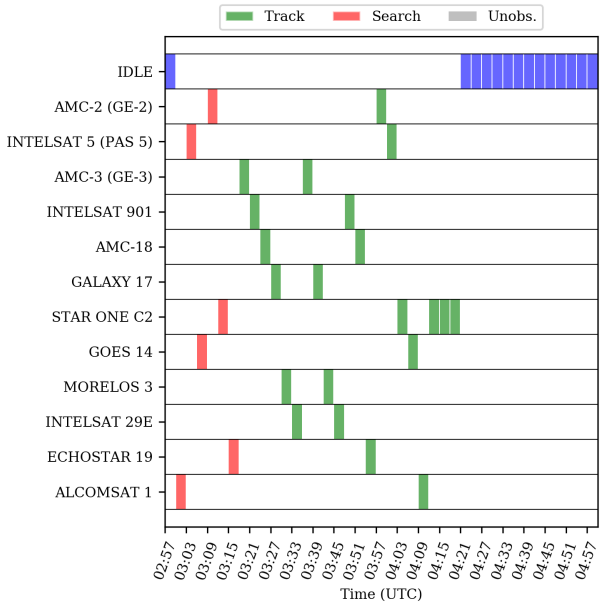

Fig. 4: Sample Simulation Telescope Schedule

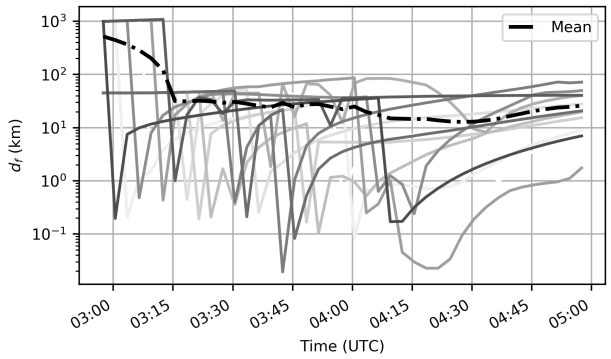

Fig. 5: Maximum reachable distances of 12 SOs over time. Mean reachable distance decreases as space objects are re-acquired by a telescope and custody is maintained.

4.2 Monte Carlo Study

Whereas the previous sections discussed one specific simulation and the results of the empirical demonstration, this section discusses the results obtained from analyzing the designed Monte Carlo experiment. A total of 201 simulations, with twelve SOs per run, are used to obtain results with the pre-defined statistical confidence level. A variety of significance levels, α, are considered for the binary detection method, directly resulting in particular probability of false alarms, p_{fa}. The overall accuracy of the algorithm, given the current BPAs and models, are summarized in Table 3. The algorithm correctly classifies, or resolves, the majority of hypotheses. This indicates the evidence to hypothesis mappings perform as designed. In general, $p_{fa} = 0.1$ resulted in the highest accuracy, though there is no clear relationship between accuracy and the chosen probability of false alarm.

Table 3: Monte Carlo Results

p_{fa}	Misclassification %	Accuracy %	Custody Maintenance %
0.05	0.0554	0.9446	100
0.10	0.0364	0.96356	100
0.15	0.0407	0.9593	100

The Monte Carlo results are also summarized through the use of confusion matrices per Monte Carlo significance level, visible in Figures 6a - 6c. Since most hypotheses are correctly resolved, the diagonal entries in the confusion matrix, which represent true positive (TP) and true negative (TN) rates are high. Enlarging the significance level α for the given binary detection method, increases the probability of false alarm for the various anomaly detections, resulting in an increase in the number of overall false-positives. This is directly visible across 6a - 6c in the lower left quadrant. Likewise, the false-negative rate decreases as the probability of false alarm is reduced, seen by the upper right quadrant. This shows the immediate trade-off between false and missed detections upon specifying a particular significance level for a binary hypothesis detection method.

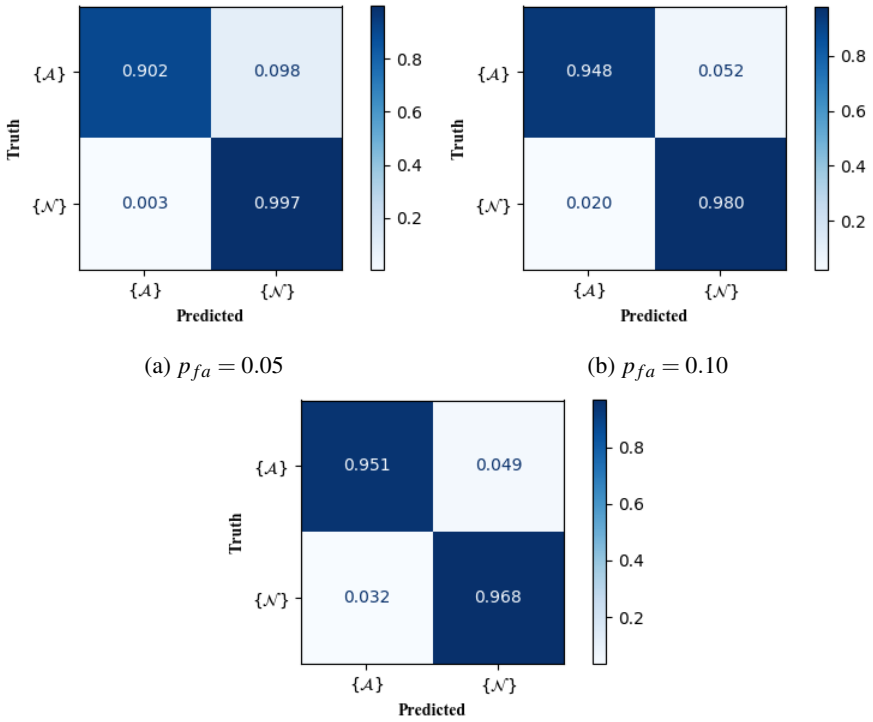

(a) $p_{fa} = 0.05$

(b) $p_{fa} = 0.10$

(c) $p_{fa} = 0.15$

Fig. 6: Confusion matrices for larger binary detection false alarm probabilities.

Discerning which probability of false alarm is preferable is contextual. There will likely be a 'best' $p_{fa} > 0$ that is a balance of false-alarm and false-negative rates. In the case of maintaining custody of spacecraft, an important aspect of SSA and SDA, higher false-negative rates may be preferred. If the true dynamical state were anomalous, and the JER algorithm discerns it to be nominal, custody would likely be lost in the future as the spacecraft will diverge from an observer's estimated trajectory. Hence, for custody maintenance, it is preferable to have higher false negative rates as a conservative measure, to ensure custody is maintained well into the future. Given the considered probabilities of false alarm, overall accuracy, and false-positive to false-negative trade-off, the intermediate $p_{fa} = 0.10$ is preferred.

4.3 Demonstration Scenario

An additional objective of this paper is to empirically validate and expand the JER algorithm's capabilities. The case and complexity to which JER is subjected relies heavily on the SOs that are considered in the experiment. The empirical validation was posed to be challenging and relevant to the SSA community at large. Many important SOs of interest lie in GEO due their cost and impact on civil and commercial infrastructure. As such, a total of 3 GEO satellites are selected, namely, ANIK G1, ANIK F2, and GOES 14. GOES 14 performs East-West station keeping maneuvers only. ANIK F2 uses continuous thrust capabilities and ANIK G1 performs North-South and East-West station keeping. These three objects are active and use different kinds of maneuvers periodically, which makes them suitable objects to consider for the anomaly and custody hypotheses.

4.4 Demonstration Results

For the purposes of the demonstration, the time-varying maximal distances, d_f, were neglected since the TLEs or nominal orbits of the GEO spacecraft were updated right before the observation campaign, resulting in very small maximal d_f. Hence, by design there never is a need to search. Instead, a static and maximum reachable set radius is used with a magnitude of $d_f = 150$ *km* for each SO. In angle-space this corresponds to a 0.24° error from a nominal orbit for GEO spacecraft. Recall that the smaller dimension of the FOV of the telescope is 16.98 arcmin $= 0.283^\circ$, thus the spacecraft reachable sets are fully contained in the telescope's FOV at all times over the course of the demonstration.

The obtained results are from an observation campaign on October 30, 2018, during Atlanta's GEO glint season, providing adequate conditions to detect and track GEO satellites. A time-horizon of two hours is given to the JER

algorithm, though the algorithm was able to resolve the hypotheses in less than an hour. The action intervals are fixed and 3 minutes long. A total of 16 actions are taken in the demonstration, totaling up to 48 minutes of observation time. Every satellite is resolved as nominal since the deviations with respect to their nominal trajectories are small in magnitude. The results from the GM-PHD filter tracking ANIK F2, GOES 14, and ANIK G1 are visible in Figures 7a -7c. Blue squares, if any, are SOs that the GM-PHD multi-target tracking algorithm monitors frame to frame but are not associated to the SO of interest, which is shown by the red square.

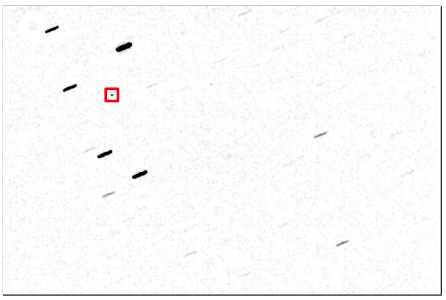

(a) Inverted Image of the Telescope FOV. GM-PHD Tracking ANIK F2 on Oct. 31, 2018 2:03:08 UTC.

(b) Inverted Image of the Telescope FOV. GM-PHD Tracking GOES 14on Oct. 31, 2018 2:05:35 UTC.

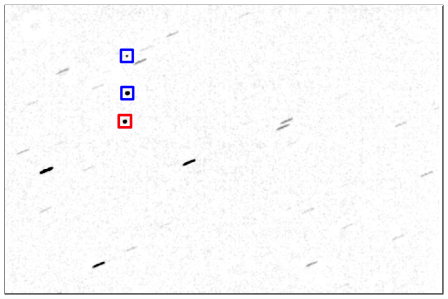

(c) Inverted Image of the Telescope FOV. GM-PHD Tracking ANIK G1 on Oct. 31, 2018 2:08:38 UTC.

Fig. 7: Anomaly and custody beliefs and plausibilities.

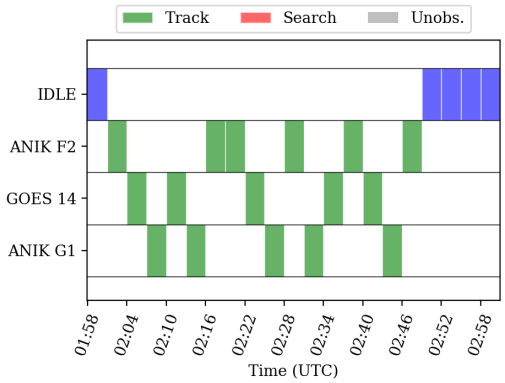

Fig. 8: GTSORT Optimal Action Sequence (Schedule)

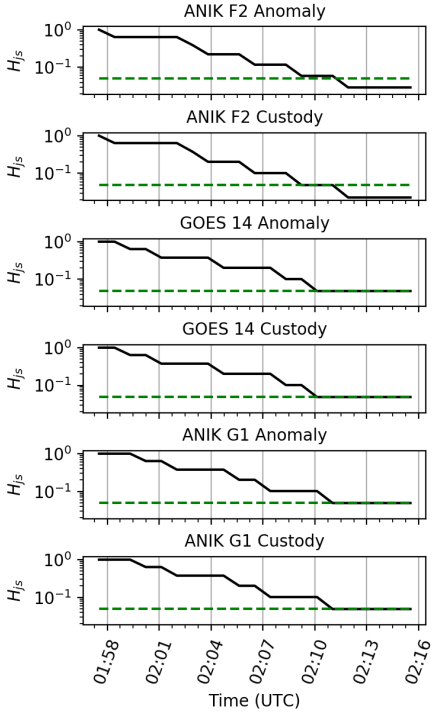

Fig. 9: Empirical demonstration hypotheses have monotonically decreasing JS entropies over the observation campaign.

As the belief in a particular proposition of the frame of discernment increases, the J-S entropy decreases, since the hypotheses are incrementally being resolved. The total uncertainty in the system, in terms of conflict and non-specificity, is being driven to zero. This suggests that a BPAs belief mass is increasingly being given to a singleton proposition in the frames of discernment, which is directly equivalent to resolving, or discerning, the true state of a hypothesis. This is also visible in Figure 9, which shows how the entropies of each hypothesis decreasing over time.

5. CONCLUSION

This paper presents novel contributions related to Dempster-Shafer theory-based telescope tasking. It applies the Judicial Evidential Reasoning framework on existing observatory hardware. A new anomaly or maneuver detection method is presented and position reachable set over-approximations are used to enforce custody of a set of space objects. Moreover, the algorithms performance and the manner in which belief is quantified is statistically analyzed by completing a Monte Carlo simulation for various detection significance levels. The results show a robust method that handles worst-case maneuver magnitudes and timing. Additionally, this methodology is implemented on a robotic telescope, showcasing the successful demonstration of the algorithm for real electro-optical sensors. Importantly, the results of this paper range from theoretical contributions to empirical ones showing a working proof of concept for hypothesis-based sensor tasking using evidential reasoning and reachability theory.

REFERENCES

[1] Travis Blake, M Sánchez, J Krassner, M Georgen, and S Sundbeck. Space domain awareness. Technical report, Defense Advanced Research Projects Agency, 2012.

[2] Grant Stokes, Curt Vo, Ramaswamy Sridharan, and Jayant Sharma. The space-based visible program. In *Space 2000 Conference and Exposition*, page 5334, 2000. doi: 10.2514/6.2000-5334.

[3] MJ Holzinger and MK Jah. Challenges and potential in space domain awareness, 2018.

[4] R Scott Erwin, Paul Albuquerque, Sudharman K Jayaweera, and Islam Hussein. Dynamic sensor tasking for space situational awareness. In *American Control Conference (ACC), 2010*, pages 1153–1158. IEEE, 2010. doi: 10.1109/ACC.2010.5530989.

[5] K. Hill, P. Sydney, K. Hamada, R. Cortez, K. Luu, M. Jah, P. Schumacher, M. Coulman, J. Houchard, and D. Naho'olewa. Covariance-based network tasking of optical sensors. In *Paper AAS 10-150 presented at the AAS/AIAA Space Flight Mechanics Conference, February*, pages 14–17, 2010.

[6] Zachary Sunberg, Suman Chakravorty, and Richard Erwin. Information space sensor tasking for space situational awareness. In *American Control Conference (ACC), 2014*, pages 79–84. IEEE, 2014. doi: 10.1109/ACC.2014.6858922.

[7] Richard Linares and Roberto Furfaro. Dynamic sensor tasking for space situational awareness via reinforcement learning. In *Advanced Maui Optical and Space Surveillance Technologies Conference*, page 36, 2016.

[8] Han Cai, Steve Gehly, Yang Yang, Reza Hoseinnezhad, Robert Norman, and Kefei Zhang. Multisensor tasking using analytical rényi divergence in labeled multi-bernoulli filtering. *Journal of Guidance, Control, and Dynamics*, pages 1–8, 2019. doi: 10.2514/1.G004232.

[9] Carolin Frueh, Hauke Fielder, and Johannes Herzog. Heuristic and optimized sensor tasking observation strategies with exemplification for geosynchronous objects. *Journal of Guidance, Control, and Dynamics*, 41(5): 1036–1048, 2017. doi: 10.2514/1.G003123.

[10] A.D. Jaunzemis, M.J. Holzinger, M.W. Chan, and P.P. Shenoy. Evidence gathering for hypothesis resolution using judicial evidential reasoning. *Information Fusion*, 49:26–45, 2019. doi: 10.1016/j.inffus.2018.09.010.

[11] Holzinger M.J. Jaunzemis, A. D. and K.K. Luu. Sensor tasking for spacecraft custody maintenance and anomaly detection using evidential reasoning. *Journal of Aerospace Information Systems*, 15(3):131–156, 2018. doi: 10.2514/1.I010584.

[12] R. Jiroušek and P.P. Shenoy. A new definition of entropy of belief functions in the dempster–shafer theory. *International Journal of Approximate Reasoning*, 92:49–65, 2018. doi: 10.1016/j.ijar.2017.10.010.

[13] Glenn Shafer. *A Mathematical Theory of Evidence*, volume 42. Princeton University Press, 1976.

[14] Arthur P Dempster. Upper and lower probabilities induced by a multivalued mapping. In *Classic Works of the Dempster-Shafer Theory of Belief Functions*, pages 57–72. Springer, 2008. doi: 10.1007/978-3-540-44792-4_3.

[15] Andris D Jaunzemis, Midhun V Mathew, and Marcus J Holzinger. Control cost and mahalanobis distance binary hypothesis testing for spacecraft maneuver detection. *Journal of Guidance, Control, and Dynamics*, pages 2058–2072, 2016. doi: 10.2514/1.G001616.

[16] E.A. Wan and R. Van Der Merwe. The unscented kalman filter for nonlinear estimation. In *Adaptive Systems for Signal Processing, Communications, and Control Symposium 2000. AS-SPCC. The IEEE 2000*, pages 153–158. Ieee, 2000. doi: 10.1109/ASSPCC.2000.882463.

[17] M.J. Holzinger and D. J. Scheeres. Reachability results for nonlinear systems with ellipsoidal initial sets. *IEEE Transactions on Aerospace and Electronic Systems*, 48(2):1583–1600, 2012. doi: 10.1109/TAES.2012.6178080.

[18] Marcus J Holzinger and Daniel J Scheeres. Reachability set subspace computation for nonlinear systems using sampling methods. In *2011 50th IEEE Conference on Decision and Control and European Control Conference*, pages 7317–7324. IEEE, 2011. doi: 10.1109/CDC.2011.6160728.

[19] Ryan D Coder and Marcus J Holzinger. Multi-objective design of optical systems for space situational awareness. *Acta Astronautica*, 128:669–684, 2016. doi: 10.1016/j.actaastro.2016.07.008.

[20] David Vallado, Paul Crawford, Ricahrd Hujsak, and TS Kelso. Revisiting spacetrack report# 3. In *AIAA/AAS Astrodynamics Specialist Conference and Exhibit*, page 6753, 2006. doi: 10.2514/6.2006-6753.

[21] Douglas C Montgomery and George C Runger. *Applied Statistics and Probability for Engineers*. John Wiley & Sons, 2010.

[22] D. Aguilar Marsillach, S. Virani, M. Holzinger, M. Chan, and P. Shenoy. Real-time telescope tasking for custody and anomaly resolution using judicial evidential reasoning. In *29th Space Flight Mechanics Symposium*. AAS, 2019.

[23] Daniel Aguilar Marsillach, Shahzad Virani, and Marcus J Holzinger. Real-time hardware-in-the-loop hand-off from a finder scope to a larger telescope, 2017.

[24] B. Vo and W. Ma. The gaussian mixture probability hypothesis density filter. *IEEE Transactions on signal processing*, 54(11):4091–4104, 2006. doi: 10.1109/TSP.2006.881190.